Chemical Science

ROYAL SOCIETY OF CHEMISTRY

EDGE ARTICLE

View Article Online
View Journal | View Issue

Cite this: *Chem. Sci.*, 2023, **14**, 4426

All publication charges for this article have been paid for by the Royal Society of Chemistry

Received 11th December 2022
Accepted 28th March 2023

DOI: 10.1039/d2sc06825g

rsc.li/chemical-science

Lemniscular carbon nanohoops with contiguous conjugation from planar chiral [2.2] paracyclophane: influence of the regioselective synthesis on topological chirality†

Jing He,[a] Mo-Han Yu,[b] Zhe Lian,[a] Yan-Qing Fan,[a] Sheng-Zhu Guo,[a] Xiao-Nan Li,[a] Ying Wang,[a] Wen-Guang Wang,[a] Zhi-Yun Cheng[c] and Hua Jiang *[a]

We report herein the regioselective synthesis of all-carbon lemniscular nanohoops ***bis-po*-CC** and ***bis-pm*-TC** by the rational control of ring closures at the different positions of planar chiral tetrasubstituted [2.2] paracyclophane. Topological analyses reveal that ***bis-pm*-TC** is topologically chiral while ***bis-po*-CC** is topologically achiral. X-ray crystal analysis demonstrates that ***bis-pm*-TC** adopts a lemniscular conformation with a contiguous conjugation. CD and CPL measurements further reveal that the chiroptical properties of ***bis-pm*-TC** are obviously different from those of ***bis-po*-CC** due to their different topological chiralities.

Introduction

Molecular architectures with fascinating topological chirality have attracted considerable attention because of their aesthetic appeal, synthetic challenge,[1] and potential applications in electronic devices[2] and molecular machines.[3] Compared to Euclidean chiral molecules having the classical stereogenic units such as points, axes, helicenes and planes, topologically chiral molecules require that their mirror image presentations are topologically distinct. Therefore, it is necessary to have nonplanar molecular graphs which cannot be converted into their mirror images by continuous deformation in 3D space without cutting.[1,4] Over the past few decades, the synthesis of topologically chiral molecules has long been dominated by mechanically interlocked molecules (MIMs),[1,5] which were conventionally synthesized by means of several reversible interactions such as active-metal templates, metal-ion templates, electrostatic interactions, π–π stacking or hydrogen bonding,[6] thus resulting in non-conjugated MIMs. In sharp contrast, synthesis of conjugated all-carbon architectures with topological chirality remains largely unexplored due to their synthetic challenge and structural complexity. Limited examples of conjugated carbon nanohoops with Möbius topology have been developed so far.[7] Therefore, there is a huge demand for developing novel strategies for accessing topologically chiral all-carbon macrocycles with aesthetic structural features, and eventually distinctive applications as functional nanocarbon materials.

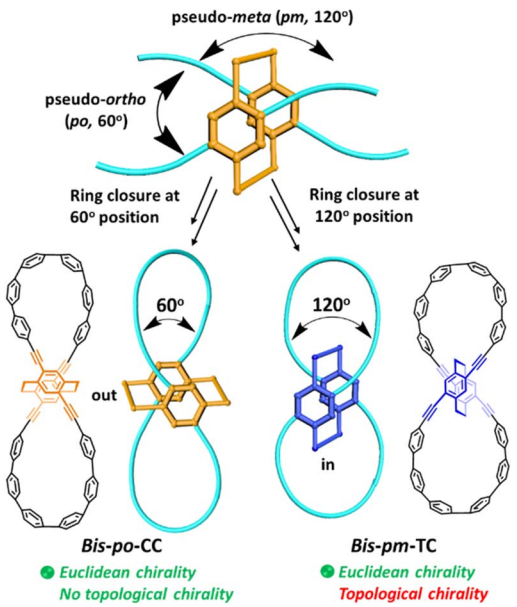

Scheme 1 Cartoon illustrations of regioselective synthesis of isomers ***bis-po*-CC** (CC = classical chirality) and ***bis-pm*-TC** (TC = topological chirality) with a differently oriented [2.2]PCP core in which the ethylene bridges are located out of and in the lemniscular framework, respectively.

[a]*College of Chemistry, Beijing Normal University, Beijing 100875, P. R. China. E-mail: jiangh@bnu.edu.cn*

[b]*College of Chemistry and Chemical Engineering, Liaoning Normal University, Dalian 116029, P. R. China*

[c]*School of Mathematical Sciences, Beijing Normal University, Beijing 100875, P. R. China*

† Electronic supplementary information (ESI) available. CCDC 2173517 and 2173519. For ESI and crystallographic data in CIF or other electronic format see DOI: https://doi.org/10.1039/d2sc06825g

The rapid development of cycloparaphenylenes (CPPs)[8] provides an excellent platform for developing topological conjugated nanocarbons. To date, a few elegant examples of CPP-based "figure-eight" or lemniscular conjugated architectures have been developed by introducing 3D covalent building blocks such as pentiptycene,[9a] bicarbazole,[9b,c] spirobifluorene,[9d] biphenyl,[9e] and tetraphenylbenzene[9f] units into the CPP backbone. Those obtained conjugated macrocycles are Euclidean chiral, but no finding on topological chirality has been disclosed.[9] Remarkably, Itami *et al.* recently reported the first synthesis of a topologically chiral all-benzene trefoil knot from CPPs by using a 3D spirosilane-assisted traceless synthetic method.[10]

Inspired by significant advances on CPP derived architectures, we envisioned a straightforward approach by introducing a chiral 3D building block into CPP backbones to design topologically chiral lemniscular carbon nanohoops. To this end, 4,7,12,15-tetrasubstituted [2.2]paracyclophane (PCP) is considered as a promising chiral 3D candidate because its diverse substituent positions and unique planar chirality[11] allow us to fulfill regioselective synthesis and to control the topological chirality of targeted nanohoops. However, none of the PCP-based macrocycles reported so far dealt with topological chirality,[12] including our previously reported semi-macrocycles **PCP-[n]CPP**,[12e] which are also topologically trivial (*vide infra*, Fig. S2†). Specifically, planar chiral 4,7,12,15-tetrasubstituted [2.2]PCP demonstrates a 60° orientation between pseudo-*ortho*(*po*) substituents and a 120° orientation between pseudo-*meta*(*pm*) substituents (Scheme 1). The obviously different orientations thus provide an appealing option to synthesize lemniscular nanohoops ***bis-po*-CC** and ***bis-pm*-TC** by regioselective ring closures (Scheme 1 and 2), leading to formation of a lemniscular framework with a differently orienting [2.2]PCP core. In detail, the ethylene bridges of the [2.2]PCP core in ***bis-po*-CC** are located out of the lemniscular framework, while those in ***bis-pm*-TC** are encircled by the lemniscular framework, reminiscent of interlocked conformations in MIMs (Scheme 1). Herein, we report the regioselective synthesis of isomers ***bis-po*-CC** and ***bis-pm*-TC** by the rational control of ring closures (Scheme 1 and 2) and our efforts to analyse the influence of regioselective synthesis on their topological chirality *via* molecular graphs obtained by Kauffman's approach (Fig. 2, *vide infra*). We found that the regioselective synthesis exerts a significant influence on the topological chirality of ***bis-pm*-TC** and ***bis-po*-CC**.

Results and discussion

Unlike the most classic topologically chiral molecules such as trefoil knots, whose topology and molecular graph are intuitional and canonical, those of ***bis-po*-CC** and ***bis-pm*-TC** are not, and thus their topological chiralities need to be detected by means of topological analysis. In this context, we utilized the topological approach proposed by L. Kauffman,[13] and further developed by E. Flapan[1b] to analyse the topological chirality of ***bis-po*-CC** and ***bis-pm*-TC**. Kauffman defined an invariant which could be used for detecting the topological chirality of rigid vertex embedded graphs. For an embedded four-valent rigid vertex graph G, C(G) is the collection of knots and links associated with G by replacing all of the vertex disks and the four strands emanating from them with each one of the four pictures on the right hand side of Fig. 1a. Kauffman proved that the set C(G) is a topological invariant of any embedded rigid vertex graph G.[13] Accordingly, if there is a topologically chiral element of C(G) that cannot be deformed to the mirror image of any other element of C(G), then G is topologically chiral. A rigid vertex embedded graph (G1) was taken as an example shown in Fig. 1b, whose C(G1) was defined to be the collection of knots and links associated with G1 by replacing the rigid vertex with each one of the four pictures on the right side of Fig. 1a. The elements of C(G1) as shown in Fig. 1b contain a trefoil knot but without its mirror image. Therefore, the rigid vertex embedded graph (G1) is topologically chiral. Lately, Flapan developed Kauffman's topological approach by treating a four substituted benzene ring as the vertex disk and created an imaginary molecule in the form of Fig. 1c. Accordingly, the benzene ring would act as a rigid vertex disk, and as such the graph would be topologically chiral because it contains a trefoil knot but not its mirror image.[1b]

Based on the aforementioned topological approach, in which the tetrasubstituted benzene ring acts as a four-valent rigid vertex disk (Fig. 1b), we first address how to detect the topological chirality of ***bis-po*-CC** and ***bis-pm*-TC**. So the tetrasubstituted benzene ring of ***bis-po*-CC** and ***bis-pm*-TC** can be replaced by each of the four pictures (I/II/III/IV) in the four-valent rigid vertex disk, respectively, as shown in Fig. 1b. We take the topological transformation of R_P-***bis-pm*-TC** into a left-handed trefoil knot graph as an example to illustrate this topological approach as shown in Fig. 2a. The carbon nanohoop R_P-***bis-pm*-TC** is reducible to graph **Rp-1**. The top benzene can be moved to the right to generate graph **Rp-2** containing two alternating crossings. In graph **Rp-2**, the left benzene ring is rotated 90° clockwise, while the right one is rotated anticlockwise to generate graph **Rp-3**. Subsequently, by replacing benzene rings **B1** and **B2** with the pictures I and IV in Fig. 1a, respectively, the graphs **Rp-4** and **Rp-4'** are obtained easily and topologically equivalent to a left-handed trefoil knot. The remaining graphs of ***bis-pm*-TC** can be obtained by a similar topological approach, and are depicted in Fig. S3.† All topologically trivial and nontrivial graphs of R_P-***bis-pm*-TC** are summarized in Table 1. Pleasingly, no right-handed trefoil knot is found in all graphs for R_P-***bis-pm*-TC**, indicating that R_P-***bis-pm*-TC** is topologically chiral. Similarly, S_P-***bis-pm*-TC** contains only a right-handed trefoil knot graph but not its mirror image and thus is topologically chiral (Fig. 2b, S4 and Table S2†). Moreover, a graph of Solomon links is also obtained for ***bis-pm*-TC**, further confirming that ***bis-pm*-TC** has topological chirality (Fig. S3†). Accordingly, the molecular graphs of the precursor ***bis-pm*-11** (Scheme 2) are the same as those of ***bis-pm*-TC** (figures not shown), and thus ***bis-pm*-11** is also topologically chiral. However, the topologic transformations of R_P-/S_P-***bis-po*-CC** only generate a planar graph (Fig. 2c and d), and thus no topologically chiral graph is found for ***bis-po*-CC** (Fig. S5 and Table S3†), suggesting that ***bis-po*-CC** is topologically achiral. The above topological analyses clearly demonstrate that the orientations of the 4,7,12,15-tetrasubstituted [2.2]PCP core

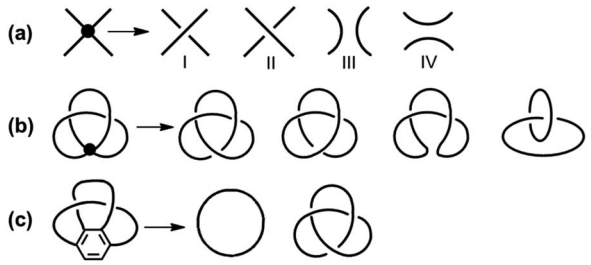

Fig. 1 (a) The construction of the set C(G) for the given rigid vertex on the left. (b) A rigid vertex embedded graph (G1) and the set C(G1) (on the right side) obtained by Kauffman's topological approach. (c) Flapan's imaginary molecule in which the benzene ring acts as a four-valent rigid vertex disk and its molecular graphs (on the right side).

resulting from the regioselective synthesis in the lemniscular conformation play a vital role in controlling the topological chirality of conjugated carbon nanohoops.

With the results from topological analysis in hand, we next set about synthesizing ***bis-po*-CC** and ***bis-pm*-TC** by regioselective synthesis (Scheme 2). For the synthesis of ***bis-po*-CC** (Scheme 2, Strategy A), we commenced with the Sonogashira–Hagihara coupling reaction with compounds ***bis-po*-3**[14] and **1**[12e] to afford intermediate ***bis-po*-4** in 35% yield, which then underwent Yamamoto coupling to give the macrocyclic precursor ***bis-po*-5** (in 37% yield) as the dominant product in which the ring closures occurred at the pseudo-*ortho* position of [2.2]PCP. Unsurprisingly, no product with the ring closures at the pseudo-*meta* position was detected and isolated due to the larger distance for ring closure at this position. The final reductive aromatization was carried out using a freshly prepared H_2SnCl_4 solution, providing ***bis-po*-CC** as a yellow solid in 40% yield.

In order to synthesize ***bis-pm*-TC**, we adopted step-wise ring closures at the pseudo-*meta* positions of 4,15-bis[(trimethylsilyl) ethynyl]-7,12-bis[(triisopropylsilyl) ethynyl] [2.2]PCP (Scheme 2: Strategy B) obtained by selective deprotection of TMS/TIPS-ethynyl groups. First, TMS groups in ***bis-pm*-5** were selectively removed by K_2CO_3/MeOH to obtain4,15-bis(ethynyl)-7,12-bis(TIPS-ethynyl) [2.2]PCP and then underwent Sonogashira–Hagihara coupling with **1** to generate ***bis-pm*-7**, which was further converted to semi-macrocyclic intermediate ***bis-pm*-8** through Yamamoto coupling. The precursor ***bis-pm*-11** was obtained by similar synthetic procedures after the deprotection of TIPS groups in ***bis-pm*-8**. The final reductive aromatization in a freshly prepared H_2SnCl_4 solution produced the desired ***bis-pm*-TC** as a yellow solid.

^{1}H-NMR spectra of ***bis-po*-CC** and ***bis-pm*-TC** reveal a sharp difference in chemical shifts of all protons (Fig. 3 and S6†). Particularly, the ^{1}H NMR spectrum of ***bis-po*-CC** shows a pair of multiplets at 3.59 and 3.04 ppm assignable to the protons of ethylene bridges and a singlet at 6.98 ppm assignable to the protons of benzene rings in the [2.2]PCP core. In contrast, the ^{1}H-NMR spectrum of ***bis-pm*-TC** displays a pair of multiplets at 2.87 and 2.58 ppm and a singlet at 6.84 ppm belonging to the protons of ethylene bridges and benzene rings, respectively. The

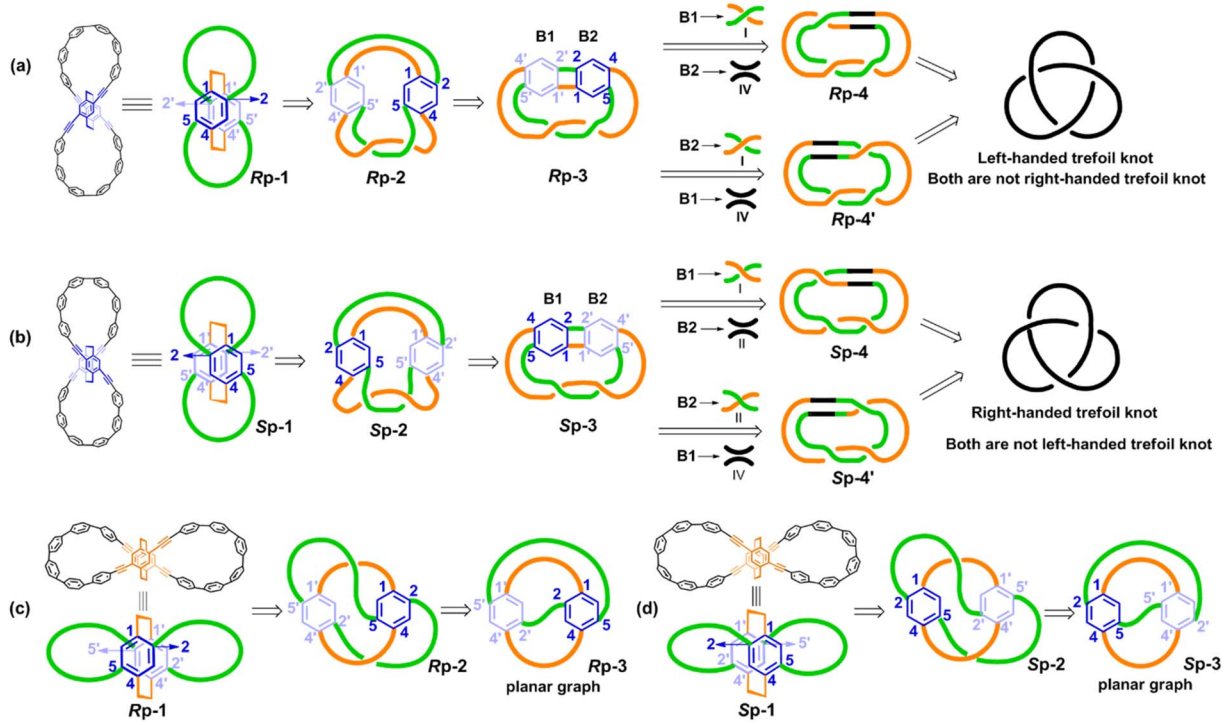

Fig. 2 Topological analyses: (a and b) representative topological transformations of R_P-***bis-pm*-TC** and S_P-***bis-pm*-TC** into the left- and right-handed trefoil knot graphs, respectively. (c and d) Representative topological transformation of R_P-***bis-po*-CC** and S_P-***bis-po*-CC** into the planar graphs.

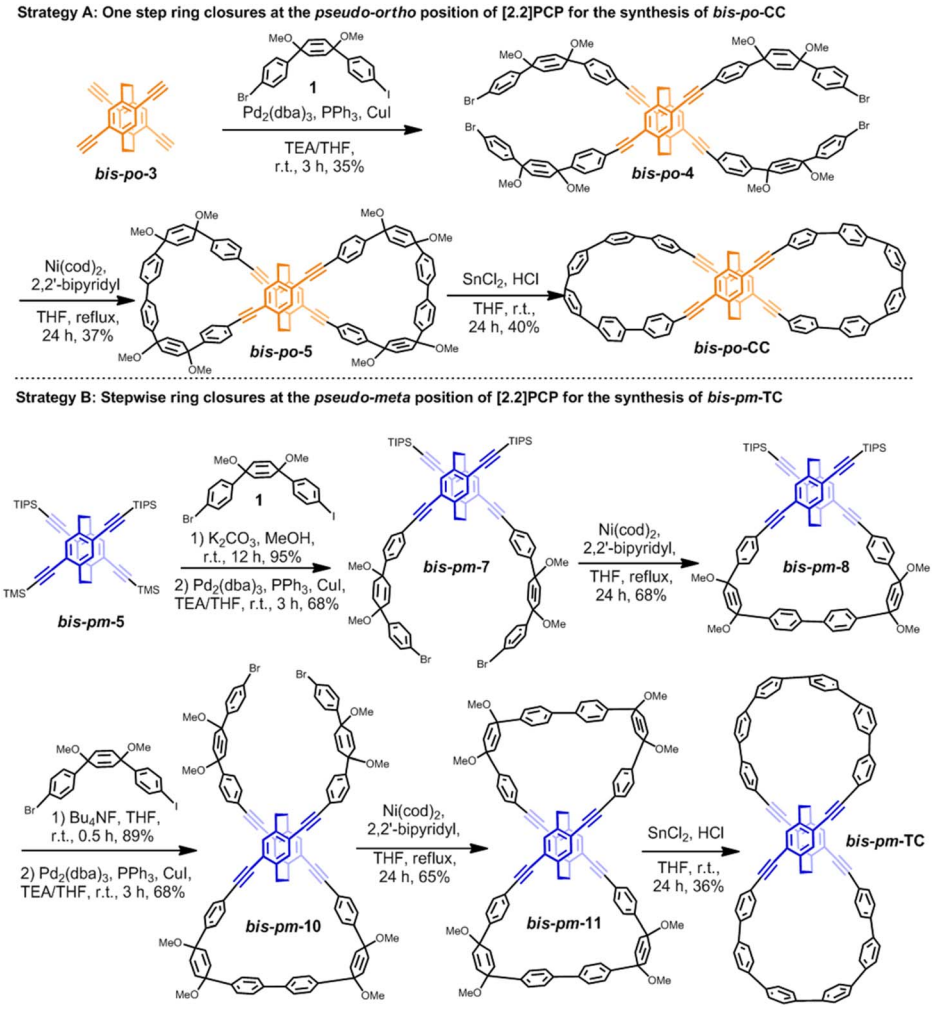

Scheme 2 Regioselective synthesis of isomers *bis-po*-CC and *bis-pm*-TC.

Table 1 All topologically trivial and nontrivial species of R_P-*bis-pm*-TC

B2 \ B1	I	II	III	IV
I				
II				
III				
IV				

data demonstrate that the protons of ethylene bridges in ***bis-pm*-TC** display significant upfield chemical shifts with $\Delta\delta$ up to 0.72 ppm in comparison with those in ***bis-po*-CC**. The significant upfield shifts of the protons of ethylene bridges can be interpreted as the shielding effects from lemniscular nanohoops (Scheme 1 and 2).

The X-ray crystallographic analysis of single crystals of ***bis-pm*-11** and ***bis-pm*-TC**, obtained by the slow vapor diffusion of hexane into a $CHCl_3$ solution at room temperature, gave unequivocal confirmation of their topological structures. The structural analysis revealed that ***bis-pm*-11** shows a bow-shaped

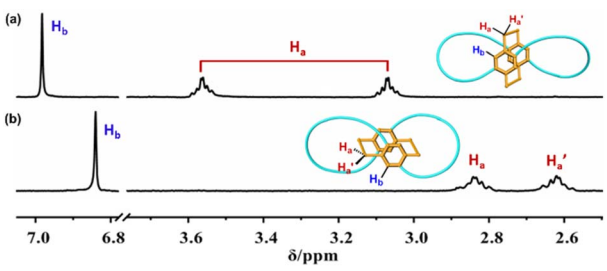

Fig. 3 Comparison of the ^{1}H NMR spectra (600 MHz, $CDCl_3$, 298 K) of (a) *bis-po*-CC and (b) *bis-pm*-TC.

conformation (Fig. 4a). Its unit cell is triclinic with a space group of $P\bar{1}$ with two opposite enantiomers in a crystal cell (Fig. S11†). The enantiomers of ***bis-pm*-11** adopt an interlaced network in the solid state (Fig. 4b). The crystal analysis revealed that ***bis-pm*-TC** adopts a twisted lemniscular structure (Fig. 4c). The unit cell is monoclinic with a space group of $P2_1/n$. Examination of the solid-state packing of ***bis-pm*-TC** reveals the ordered supramolecular alignment of long-channels (Fig. 4d). Many attempts to grow suitable crystals of ***bis-po*-CC** failed.

The photophysical properties of ***bis-po*-CC** and ***bis-pm*-TC** were investigated in dichloromethane solutions (Fig. 5). The absorption spectrum of ***bis-po*-CC** exhibits two major absorption peaks at 334 nm ($\varepsilon = 2.5 \times 10^5$ M^{-1} cm^{-1}) and 361 nm ($\varepsilon = 2.4 \times 10^5$ M^{-1} cm^{-1}), which are ascribed to the electronic transitions of HOMO−2 → LUMO+2 ($\lambda_{DFT} = 328$ nm) and HOMO−2 → LUMO ($\lambda_{DFT} = 367$ nm), respectively, according to time-dependent density functional theory (TD-DFT) calculations (Fig. S18 and Table S9†). In contrast, ***bis-pm*-TC** shows only one intense absorption band at 338 nm ($\varepsilon = 2.7 \times 10^5$ M^{-1} cm^{-1}) correlating with the transitions of HOMO → LUMO and HOMO−2 → LUMO+1 ($\lambda_{DFT} = 341$ nm) (Fig. S19 and Table S11†).

The fluorescence emission spectrum of ***bis-po*-CC** exhibits one emission band with a maximum peak at 495 nm under excitation at 330 nm (Fig. 5), while the emission spectrum of ***bis-pm*-TC** shows a slight blueshift feature with a maximum peak at 484 nm. It is worth noting that these emission peaks obviously shifted towards lower energy in comparison with their semi-macrocycle ***pm*-PCP-[6]CPP** ($\lambda_{em} = 472$ nm),[12e] indicative of a contiguous conjugation in the lemniscular conformations. The fluorescence quantum yields of ***bis-po*-CC** and ***bis-pm*-TC** were determined to be 33% and 51%, respectively. In addition, the fluorescence lifetimes (τ) of ***bis-po*-CC** and ***bis-pm*-TC** were calculated to be 2.4 and 3.2 ns, respectively, fitting with a single exponential relationship (Fig. S15†).

The enantiomers of ***bis-po*-CC** and ***bis-pm*-TC** were separated by chiral HPLC (Fig. S13 and S14†), respectively, and their CD spectra are depicted in Fig. 6a. The absolute configurations of the

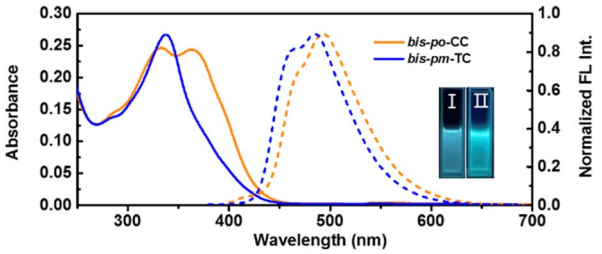

Fig. 5 UV-vis absorption (solid lines) and fluorescence (dashed lines) spectra of ***bis-po*-CC** and ***bis-pm*-TC** in dichloromethane ($c = 1.0 \times 10^{-5}$ M). Photograph showing the fluorescence of ***bis-po*-CC**(I), and ***bis-pm*-TC**(II) under 365 nm using a UV lamp (inset).

enantiomers were assigned according to TD-DFT calculations (Fig. S20†). The CD spectra of enantiomers ***bis-po*-CC** and ***bis-pm*-TC** feature bands with variable intensities between 250 and 450 nm with a maximum at 393 nm ($|\Delta\varepsilon| = 54$ M^{-1} cm^{-1}) for ***bis-po*-CC** and at 337 nm ($|\Delta\varepsilon| = 57$ M^{-1} cm^{-1}) for ***bis-pm*-TC** (Fig. 6a). The CD spectrum of R_P-***bis-po*-CC** shows the positive of negative sign for any given wavelength. Interestingly, the CD spectrum of R_P-***bis-pm*-TC** displays bands with an inverted sign, suggesting a chirality opposite to that of R_P-***bis-po*-CC** even though they contain the same planar chiral R_P-[2.2] PCP core. The inverted sign can be interpreted as the different orientations of the [2.2] PCP core in the lemniscular carbon nanohoops and as the topological chirality of R_P-***bis-pm*-TC**. The CD spectra of S_P-enantiomers exhibit the mirror images of those of R_P-ones for both carbon nanohoops. The dissymmetry factors $|g_{abs}| = |\Delta\varepsilon/\varepsilon|$ were calculated to be 3.1×10^{-3} (390 nm) for ***bis-po*-CC** and 2.9×10^{-3} (387 nm) for ***bis-pm*-TC**. The circularly polarized luminescence (CPL) spectra reveal that R_P-***bis-po*-CC** shows one positive CPL signal in the range of 400–700 nm, whereas R_P-***bis-pm*-TC** displays one negative signal in the same region (Fig. 6b), consistent with the observations from the ECD results. Similarly, the CPL spectra of S_P- enantiomers exhibited the mirror images of those of R_P-ones. The CPL dissymmetry factor ($|g_{lum}|$) was

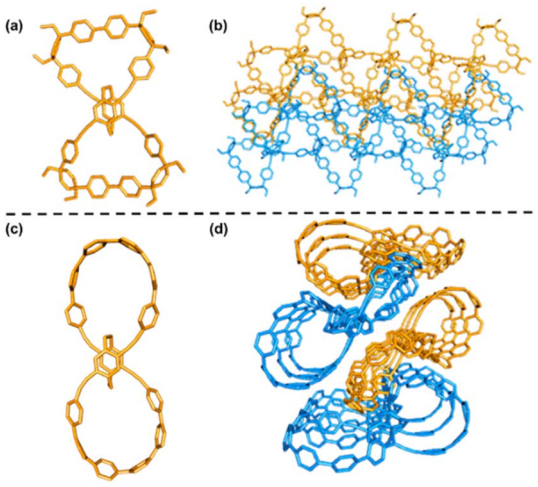

Fig. 4 X-ray crystal structures of the bow-shaped ***bis-pm*-11** (a) and its crystal packing (b). X-ray crystal structures of the figure-eight shaped ***bis-pm*-TC** (c) and its crystal packing (d).

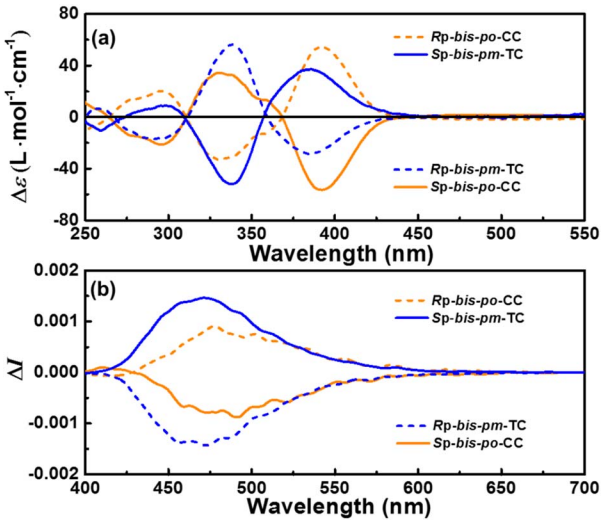

Fig. 6 (a) CD and (b) CPL spectra of ***bis-po*-CC** and ***bis-pm*-TC** in dichloromethane ($c = 1.0 \times 10^{-5}$ M).

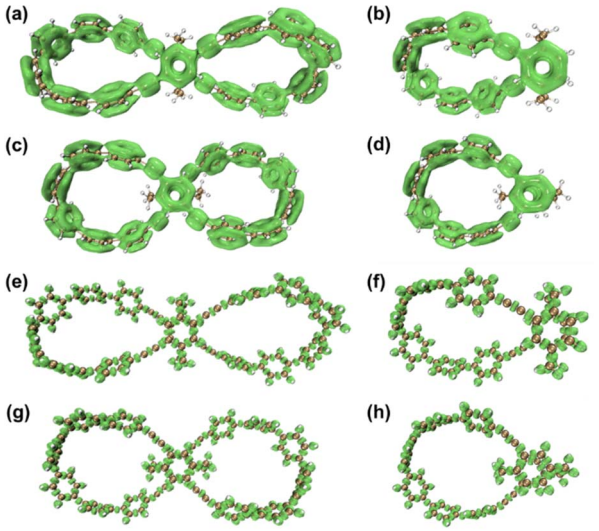

Fig. 7 (a) LOL-π isosurfaces (isovalue = 0.30) for (a) ***bis-po*-CC**, (b) ***po*-PCP-[6]CPP**, (c) ***bis-pm*-TC** and (d) ***pm*-PCP-[6]CPP** and LOL-σ (isovalue = 0.60) for (e) ***bis-po*-CC**, (f) ***po*-PCP-[6]CPP**, (g) ***bis-pm*-TC** and (h) ***pm*-PCP-[6]CPP**.

determined as 1.8×10^{-3} at 491 nm for ***bis-po*-CC** and 3.2×10^{-3} at 472 nm for ***bis-pm*-TC**, respectively. The larger $|g_{lum}|$ value for ***bis-pm*-TC** might be ascribed to the more rigid structure of ***bis-pm*-TC** in the excited state.[12e] Moreover, the $|g_{lum}|$ values are comparable with those of most of the CPL-active small organic molecules, which are typically in the range of 10^{-2} to 10^{-4} (Fig. S16 and Table S6†).[15] However, it is very challenging to differentiate topological chirality from chemical one in ***bis-pm*-TC** by experimental methods because the nanohoop contains a classic stereogenic motif. Such challenges also exist in other reported topologically chiral MIMs and organic trefoil knots.[16]

The localized orbital locator (LOL)[17] provides an intuitive depiction of isolated electron densities of π-electrons. The LOL isosurfaces of semi-macrocycles ***po*-PCP-[6]CPP** and ***pm*-PCP-[6]CPP** were calculated for comparison with lemniscular nanohoops ***bis-po*-CC** and ***bis-pm*-TC**. In the case of ***bis-po*-CC** and ***bis-pm*-TC**, contiguously delocalized π-electron density is accumulated in all benzene rings at LOL-π isovalue = 0.30 level (Fig. 7). At the same isovalue level, for the semi-macrocycle, the π-electrons also delocalize over almost all the benzene rings including the [2.2] PCP core (Fig. S22†). However, LOL-π investigations revealed a contiguously circular conjugation for both ***bis-po*-CC** and ***bis-pm*-TC** with a lemniscular framework but an acyclic conjugation for semi-macrocycles ***po*/*pm*-PCP-[6]CPP**, indicative of a larger extent of delocalization for the former. The same arguments also hold for LOL-σ plots at isovalue = 0.60 for all nanohoops (Fig. 7 and S23†). The LOL investigations are in good agreement with the results of the redshift in fluorescence emission.

Data availability

Data available in the ESI.†

Conclusions

In conclusion, we have reported the regioselective synthesis of lemniscular carbon nanohoops ***bis-po*-CC** and ***bis-pm*-TC** by the judicious control of the ring closures at the different positions of the 3D planar chiral tetrasubstituted [2.2]PCP. The topological analysis demonstrated that ***bis-pm*-TC** is topologically chiral but ***bis-po*-CC** not. Interestingly, CD and CPL experiments revealed that chiral isomers $R_P(S_P)$-***bis-po*-CC** and $R_P(S_P)$-***bis-pm*-TC** exhibited opposite chiral signals even though they contain the same planar chiral $R_P(S_P)$-[2.2] PCP cores in the lemniscular nanohoops. This unique phenomenon originates from the different orientations of the imbedded [2.2] PCP core in the lemniscular nanohoops and their different topological chiralities. This work provides a new guideline for design and synthesis of topologically chiral all-carbon molecules.

Author contributions

J. H. synthesized and characterized all materials. M.-H. Y. performed DFT calculations and simulations of photophysical spectra. Z. L. and Y.-Q. F. collected X-ray data. S.-Z. G. and X.-N. L synthesized partial material. Y. W. performed DFT calculations of LOL isosurfaces. W.-G. W. helped to analyze some of the experimental data. Z.-Y. C. gave guidance about the topological analyses. H. J. supervised this project and revised the manuscript. All authors have given approval to the final version of the manuscript.

Conflicts of interest

There are no conflicts to declare.

Acknowledgements

This work was financially supported by the Beijing Natural Science Foundation (2212008) and the National Natural Science Foundation of China (21971020 and 22271019).

References

1 (*a*) *Molecular Catenanes, Rotaxanes and Knots*, ed. J.-P. Sauvage and C. Dietrich-Buchecker, Wiley-VCH, Weinheim, Germany, 1999; (*b*) *When Topology Meets Chemistry: A Topological Look at Molecular Chirality*, ed. E. Flapan, Cambridge University Press, Cambridge, England, 2000; (*c*) F. Vögtle and O. Lukin, *Angew. Chem., Int. Ed.*, 2005, **44**, 1456; (*d*) R. S. Forgan, J.-P. Sauvage and J. F. Stoddart, *Chem. Rev.*, 2011, **111**, 5434.

2 A. Coskun, J. M. Spruell, G. Barin, W. R. Dichtel, A. H. Flood, Y. Y. Botros and J. F. Stoddart, *Chem. Soc. Rev.*, 2012, **41**, 4827.

3 (*a*) S. Erbas-Cakmak, D. A. Leigh, C. T. McTernan and A. L. Nussbaumer, *Chem. Rev.*, 2015, **115**, 10081; (*b*) J.-P. Sauvage, *Angew. Chem., Int. Ed.*, 2017, **56**, 11080.

4 (*a*) H. L. Frisch and E. Wasserman, *J. Am. Chem. Soc.*, 1961, **83**, 3789; (*b*) D. M. Walba, *Tetrahedron*, 1985, **41**, 3161; (*c*)

D. K. Mitchell and J.-P. Sauvage, *Angew. Chem., Int. Ed.*, 1988, **27**, 930; (*d*) J. C. Chambron, C. O. Dietrich-Buchecker and J.-P. Sauvage, *Top. Curr. Chem.*, 1993, **165**, 132; (*e*) C. Liang and K. Mislow, *J. Am. Chem. Soc.*, 1994, **116**, 3588; (*f*) C. Dietrich-Buchecker, G. Rapenne, J.-P. Sauvage, A. De Cian and J. Fischer, *Chem. – Eur. J.*, 1999, **5**, 1432.

5 For selected reviews, see: (*a*) F. M. Raymo and J. F. Stoddart, *Chem. Rev.*, 1999, **99**, 1643; (*b*) J. F. Stoddart, *Chem. Soc. Rev.*, 2009, **38**, 1802; (*c*) G. Gil-Ramírez, D. A. Leigh and A. J. Stephens, *Angew. Chem., Int. Ed.*, 2015, **54**, 6110; (*d*) S. D. P. Fielden, D. A. Leigh and S. L. Woltering, *Angew. Chem., Int. Ed.*, 2017, **56**, 11166; (*e*) E. M. G. Jamieson, F. Modicom and S. M. Goldup, *Chem. Soc. Rev.*, 2018, **47**, 5266; (*f*) S. Mena-Hernando and E. M. Pérez, *Chem. Soc. Rev.*, 2019, **48**, 5016.

6 (*a*) J. C. Chambron and J.-P. Sauvage, *New J. Chem.*, 2013, **37**, 49; (*b*) J.-F. Ayme, J. E. Beves, C. J. Campbell and D. A. Leigh, *Chem. Soc. Rev.*, 2013, **42**, 1700; (*c*) *The Nature of the Mechanical Bond: From Molecules to Machines*, ed. C. J. Bruns and J. F. Stoddart, John Wiley & Sons, Inc., Hoboken, 2016; (*d*) H.-N. Zhang, W.-X. Gao, Y.-J. Lin and G.-X. Jin, *J. Am. Chem. Soc.*, 2019, **141**, 16057; (*e*) M. Denis, J. E. M. Lewis, F. Modicom and S. M. Goldup, *Chem*, 2019, **5**, 1512; (*f*) Z. Cui, Y. Lu, X. Gao, H.-J. Feng and G.-X. Jin, *J. Am. Chem. Soc.*, 2020, **142**, 13667; (*g*) J. R. J. Maynard and S. M. Goldup, *Chem*, 2020, **6**, 1914; (*h*) W.-X. Gao, H.-J. Feng, B.-B. Guo and G.-X. Jin, *Chem. Rev.*, 2020, **120**, 6288; (*i*) Q.-H. Guo, Y. Jiao, Y. Feng and J.-F. Stoddart, *CCS Chem.*, 2021, **3**, 1542; (*j*) A. Rodriguez-Rubio, A. Savoini, F. Modicom, P. Butler and S. M. Goldup, *J. Am. Chem. Soc.*, 2022, **144**, 11927; (*k*) Y. Wang, J. Gong, X. Wang, W.-J. Li, X.-Q. Wang, X. He, W. Wang and H.-B. Yang, *Angew. Chem., Int. Ed.*, 2022, **61**, e202210542.

7 (*a*) G. R. Schaller, F. Topić, K. Rissanen, Y. Okamoto, J. Shen and R. Herges, *Nat. Chem.*, 2014, **6**, 608; (*b*) G. Naulet, L. Sturm, A. Robert, P. Dechambenoit, F. Röhricht, R. Herges, H. Bock and F. Durola, *Chem. Sci.*, 2018, **9**, 8930; (*c*) S. Nishigaki, Y. Shibata, A. Nakajima, H. Okajima, Y. Masumoto, T. Osawa, A. Muranaka, H. Sugiyama, A. Horikawa, H. Uekusa, H. Koshino, M. Uchiyama, A. Sakamoto and K. Tanaka, *J. Am. Chem. Soc.*, 2019, **141**, 14955; (*d*) X. Jiang, J. D. Laffoon, D. Chen, S. Pérez-Estrada, A. S. Danis, J. Rodríguez-López, M. A. Garcia-Garibay, J. Zhu and J. S. Moore, *J. Am. Chem. Soc.*, 2020, **142**, 6493; (*e*) Y. Segawa, T. Watanabe, K. Yamanoue, M. Kuwayama, K. Watanabe, J. Pirillo, Y. Hijikata and K. Itami, *Nat. Synth.*, 2022, **1**, 535.

8 For selected reviews, see: (*a*) H. Omachi, Y. Segawa and K. Itami, *Acc. Chem. Res.*, 2012, **45**, 1378; (*b*) S. Yamago, E. Kayahara and T. Iwamoto, *Chem. Rec.*, 2014, **14**, 84; (*c*) M. R. Golder and R. Jasti, *Acc. Chem. Res.*, 2015, **48**, 557; (*d*) E. R. Darzi and R. Jasti, *Chem. Soc. Rev.*, 2015, **44**, 6401; (*e*) S. E. Lewis, *Chem. Soc. Rev.*, 2015, **44**, 2221; (*f*) Y. Segawa, A. Yagi, K. Matsui and K. Itami, *Angew. Chem., Int. Ed.*, 2016, **55**, 5136; (*g*) D. Wu, W. Cheng, X. Ban and J. Xia, *Asian J. Org. Chem.*, 2018, **7**, 2161; (*h*) M. Hermann, D. Wassy and B. Esser, *Angew. Chem., Int. Ed.*, 2021, **60**, 15743.

9 (*a*) W. Xu, X.-D. Yang, X.-B. Fan, X. Wang, C.-H. Tung, L.-Z. Wu and H. Cong, *Angew. Chem., Int. Ed.*, 2019, **58**, 3943; (*b*) K. Senthilkumar, M. Kondratowicz, T. Lis, P. J. Chmielewski, J. Cybinska, J. L. Zafra, J. Casado, T. Vives, J. Crassous, L. Favereau and M. Stępień, *J. Am. Chem. Soc.*, 2019, **141**, 7421; (*c*) L. Palomo, L. Favereau, K. Senthilkumar, M. Stępień, J. Casado and F. J. Ramírez, *Angew. Chem., Int. Ed.*, 2022, **61**, e202206976; (*d*) T. A. Schaub, E. A. Prantl, J. Kohn, M. Bursch, C. R. Marshall, E. J. Leonhardt, T. C. Lovell, L. N. Zakharov, C. K. Brozek, S. R. Waldvogel, S. Grimme and R. Jasti, *J. Am. Chem. Soc.*, 2020, **142**, 8763; (*e*) L.-H. Wang, N. Hayase, H. Sugiyama, J. Nogami, H. Uekusa and K. Tanaka, *Angew. Chem., Int. Ed.*, 2020, **59**, 17951; (*f*) X. Zhang, H. Liu, G. Zhuang, S. Yang and P. Du, *Nat. Commun.*, 2022, **13**, 3543.

10 Y. Segawa, M. Kuwayama, Y. Hijikata, M. Fushimi, T. Nishihara, J. Pirillo, J. Shirasaki, N. Kubota and K. Itami, *Science*, 2019, **365**, 272.

11 (*a*) Z. Hassan, E. Spuling, D. M. Knoll and S. Bräse, *Angew. Chem., Int. Ed.*, 2020, **59**, 2156; (*b*) J.-M. Teng, D.-W. Zhang and C.-F. Chen, *ChemPhotoChem*, 2022, **6**, e202100228.

12 Examples see: (*a*) Y. Morisaki, M. Gon, T. Sasamori, N. Tokitoh and Y. Chujo, *J. Am. Chem. Soc.*, 2014, **136**, 3350; (*b*) K. J. Weiland, T. Brandl, K. Atz, A. Prescimone, D. Haussinger, T. Solomek and M. Mayor, *J. Am. Chem. Soc.*, 2019, **141**, 2104; (*c*) Y. Wu, G. Zhuang, S. Cui, Y. Zhou, J. Wang, Q. Huang and P. Du, *Chem. Commun.*, 2019, **55**, 14617; (*d*) K. Tanaka, R. Inoue and Y. Morisaki, *Chem. – Asian J.*, 2022, **17**, e202101267; (*e*) J. He, M. Yu, M. Pang, Y. Fan, Z. Lian, Y. Wang, W. Wang, Y. Liu and H. Jiang, *Chem. – Eur. J.*, 2022, **28**, e202103832; (*f*) E. Sidler, P. Zwick, C. Kress, K. Reznikova, O. Fuhr, D. Fenske and M. Mayor, *Chem. – Eur. J.*, 2022, **28**, e202201764; (*g*) M. Hasegawa, Y. Ishida, H. Sasaki, S. Ishioka, K. Usui, N. Hara, M. Kitahara, Y. Imai and Y. Mazaki, *Chem. – Eur. J.*, 2021, **27**, 16225; (*h*) M. Tsuchiya, R. Inoue, K. Tanaka and Y. Morisaki, *Chem. – Asian J.*, 2022, **17**, e202200418.

13 (*a*) L. Kauffman, *Topology*, 1987, **26**, 395; (*b*) L. Kauffman, *Trans. Amer. Math. Soc.*, 1989, **311**, 697.

14 L. Bondarenko, I. Dix, H. Hinrichs and H. Hopf, *Synthesis*, 2004, **16**, 2751.

15 (*a*) J. Kumar, T. Nakashima and T. Kawai, *J. Phys. Chem. Lett.*, 2015, **6**, 3445–3452; (*b*) E. M. Sánchez-Carnerero, A. R. Agarrabeitia, F. Moreno, B. L. Maroto, G. Muller, M. J. Ortiz and S. de la Moya, *Chem. – Eur. J.*, 2015, **21**, 13488–13500; (*c*) J. Roose, B.-Z. Tang and K.-S. Wong, *Small*, 2016, **12**, 6495–6512; (*d*) M. Li, W.-B. Lin, L. Fang and C.-F. Chen, *Acta Chim. Sin.*, 2017, **75**, 1150–1163; (*e*) J. Han, S. Guo, H. Lu, S. Liu, Q. Zhao and W. Huang, *Adv. Opt. Mater.*, 2018, **6**, 1800538; (*f*) H. Tanaka, Y. Inoue and T. Mori, *ChemPhotoChem*, 2018, **2**, 386–402; (*g*) D. Zheng, L. Zheng, C. Yu, Y. Zhan, Y. Wang and H. Jiang, *Org. Lett.*, 2019, **21**, 2555–2559; (*h*) D. Zheng, C. Yu, L. Zheng, Y. Zhan and H. Jiang, *Chin. Chem. Lett.*, 2020, **31**, 673–676;

(*i*) F. Song, Z. Zhao, Z. Liu, J. W. Y. Lam and B.-Z. Tang, *J. Mater. Chem. C*, 2020, **8**, 3284–3301; (*j*) *Circularly Polarized Luminescence of Isolated Small Organic Molecules*, ed. T. Mori, Springer, Singapore, 2020.

16 (*a*) L. E. Perret-Aebi, A. von Zelewsky, C. D. Dietrich-Buchecker and J.-P. Sauvage, *Angew. Chem., Int. Ed.*, 2004, **43**, 4482; (*b*) A. Theil, C. Mauve, M.-T. Adeline, A. Marinetti and J.-P. Sauvage, *Angew. Chem., Int. Ed.*, 2006, **45**, 2104; (*c*) M. Feigel, R. Ladberg, S. Engels, R. Herbst-Irmer and R. Fröhlich, *Angew. Chem., Int. Ed.*, 2006, **45**, 5698; (*d*) N. Ponnuswamy, F. B. L. Cougnon, J. M. Clough, G. D. Pantos and J. K. M. Sanders, *Science*, 2012, **338**, 783.

17 (*a*) H. L. Schmider and A. D. Becke, Chemical content of the kinetic energy density, *J. Mol. Struct.: THEOCHEM*, 2000, 51–61; (*b*) J. F. Gonthier, S. N. Steinmann, L. Roch, A. Ruggi, N. Luisier, K. Severin and C. Corminboeuf, *Chem. Commun.*, 2012, **48**, 9239; (*c*) Z. Liu, T. Lu, S. Hua and Y. Yu, *J. Phys. Chem. C*, 2019, **123**, 18593.